JOURNAL OF CATALYSIS 141, 671–687 (1993)

Physicochemical Study of Structural Disorder in Vanadyl Pyrophosphate

M. LÓPEZ GRANADOS, J. C. CONESA, AND M. FERNÁNDEZ-GARCÍA

Instituto de Catálisis y Petroleoquímica, CSIC, Cantoblanco, Campus de la Universidad Autónoma, 28049 Madrid, Spain

Received June 15, 1992; revised November 3, 1992

Vanadium phosphate specimens have been prepared in aqueous or organic media following procedures typical in the preparation of catalysts for selective hydrocarbon oxidation, and the materials obtained are examined with XRD, TGA, IR, ESR, and EXAFS techniques. The results show a particular ability of the $(VO)_2P_2O_7$ structure to keep (most of the) vanadium in mixed-valence V^{IV}–V^{V} pairs, probably ordered in the lattice in a specific manner, while the corresponding excess oxygen seems to remain trapped between the layers of the structure. In spite of this nonstoichiometric character, however, XRD continues to show only the reflections of the $(VO)_2P_2O_7$ lattice. The possibility that the use of both an organic solvent and P : V ratios higher than 1 during catalyst preparation help to avoid the phenomena, possibly detrimental for catalyst operation, of deeper vanadium oxidation (beyond the mentioned mixed-valence state) and generation of faults in the P–O–P links between the layers of the $(VO)_2P_2O_7$-type structure is discussed. The possible relevance of these results for the operation of these catalysts in practical reactions is also discussed.

INTRODUCTION

The V–P–O system is a complex one, for which many phases having interesting properties (*1–5*) as ionic conductors, cathodic materials, ion exchangers, electronic anisotropic conductors, and, most especially, heterogeneous catalysts for partial oxidation of hydrocarbons are known; in particular, their main industrial application is the oxidation of C_4 hydrocarbons to maleic anhydride (*6–10*). In this case, the reaction is a structure-sensitive one, for which the best catalysts known to date are identified as the pyrophosphate phase $(VO)_2P_2O_7$, with the active centers being located at the exposed (100) planes of its layer-type structure (*11–14*). This material is usually prepared by calcination/decomposition of a precursor phase, the hemihydrate $(VO)HPO_4 \cdot \frac{1}{2}H_2O$, which in turn is obtained by precipitation in a suitable solvent. These two compounds are structurally related: Their crystalline lattices (Fig. 1) can be described in both cases as built from vanadyl pairs, with the vanadium coordination shaped in distorted octahedra that share, in each pair, one edge (in the case of $(VO)_2P_2O_7$) or one face (in the case of $VOHPO_4 \cdot \frac{1}{2}H_2O$). These octahedron pairs are connected to each other by phosphate links, forming infinite layers oriented perpendicularly to the z axis in $(VO)HPO_4 \cdot \frac{1}{2}H_2O$ and to the x axis in $(VO)_2P_2O_7$. In the first case, these layers accommodate water molecules between them and are held together by hydrogen bonds, while in the second case they are bonded covalently by the pyrophosphate P–O–P links, which are oriented roughly perpendicular to the layers. It is usually recognized that the thermal transformation of $(VO)HPO_4 \cdot \frac{1}{2}H_2O$ into $(VO)_2P_2O_7$ proceeds via a topotactic dehydration mechanism (*15–18*).

The activity of this catalyst depends markedly on its method of preparation, the most active material being obtained through an organic solvent-based procedure using initially a P : V ratio slightly higher than 1. The working catalyst may have a substantial amount of vanadium oxidized into the pen-

0021-9517/93 $5.00

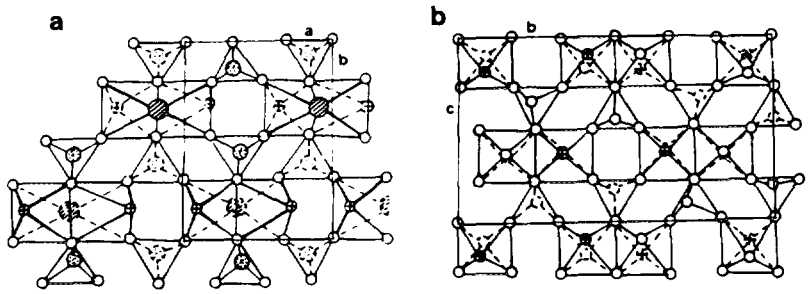

FIG. 1. Crystal structures of (a) (001) plane of $(VO)HPO_4 \cdot \frac{1}{2}H_2O$ and (b) (100) plane of $(VO)_2P_2O_7$ [from Ref. (*11*)].

tavalent state even though no recognizable V^V phase is detectable (*17–29*). The structure of this catalytic material at the molecular level and its evolution during the preparation and operation stages are not yet satisfactorily clarified. The present work tries to obtain further insight into this subject by examining with several physicochemical characterization techniques different specimens of this material in the state present after preparation, i.e., before catalytic reaction. Information on the local nature of the defects corresponding to the mixed valent state of vanadium, and also on those structural and chemical properties of the material that vary when the main parameters of the preparation procedure (type of solvent, P : V ratio) are changed, has been obtained.

EXPERIMENTAL

Sample Preparation

The specimens examined were obtained following well-known procedures that use either aqueous or organic solvents. One sample was prepared as described by Centi *et al.* (*16*): 15 g of V_2O_5 were added to 200 ml of aqueous HCl (35%), and the mixture was boiled for 2 h until full dissolution of the oxide was achieved. Concentrated H_3PO_4 (85%) was then added to the cool solution, in the amount appropriate to achieving a ratio P : V = 1. The resulting liquid was concentrated by evaporation to give 15–20 ml syrup; 100 ml of boiling water was added, and the solution was left standing 24 h. The resulting precipitate was filtered and rinsed with distilled water until absence of chloride and dried in air 24 h at 395 K. The precursor thus prepared is designated here VPAQ.

Several samples were prepared in organic medium, starting with different P : V ratios and using also a typical procedure described in the literature (*6, 19, 20*): 18 g of V_2O_5 were refluxed for 24 h with 100 ml of *n*-butanol, and after cooling to room temperature, the desired amount of H_3PO_4 (dehydrated by prolonged evaporation at $T \approx$ 345 K under vacuum) was added. The mixture was refluxed for 24 h, and the resulting precipitate was filtered, washed with *n*-butanol, and dried in air as before. The samples so obtained are designated VP*x*, where *x* (= 0.7, 0.91, 1.0, 1.21) is the P : V ratio used in the initial mixture. The resulting P : V ratios in all the precursors were evaluated with SEM/EDAX measurements, yielding in all of them similar values close to 1, even in the cases where ratios much different from 1 were used in the preparation mixture; this agrees with results reported in the literature for similar preparations (*19*).

From all these precursors, calcined specimens (designated here VPAQ-C or VP*x*-C) were obtained by programmed heating under air (rate = 5 K/min) up to total dehydration of the precursor (~673 K for the organic precursors and 723 K for the aqueous precursor). Also, a well-crystallized $(VO)_2P_2O_7$

specimen was prepared by heating a portion of the VP1.0-C sample under N_2 up to 1073 K (rate = 5 K/min).

Characterization Methods

Thermogravimetric analyses were carried out at 5 K/min heating rate with a DuPont 951/990 balance/controller system. Typically, 40-mg portions of material were used, the measurement precision being ca. 5 μg. Powder X-ray diffraction diagrams were obtained in a Philips PW 1716/30 diffractometer using Cu$K\alpha$ radiation. FTIR spectra were recorded with a Nicolet 57 DX spectrometer at resolutions of 2–4 cm^{-1}, with the sample powder diluted in KBr (2%) and pressed into 13-mm diam pellets. ESR spectra were obtained using a liquid N_2 cryostat in an X-band Bruker ER 200 spectrometer interfaced to a Bruker ESP-1600 computer system; a DPPH standard was used to calibrate the g-value scale, the ESR parameters being refined by comparison with spectra generated by computer simulation (*30*). SEM/EDAX measurements were carried out on an ISI DS-130 scanning electron microscope coupled to an Si(Li) X-ray detector and a Kevex 8000II processor for energy dispersive X-ray analysis.

X-ray absorption measurements were carried out at station EXAFS III mounted in the DCI ring (1.85 GeV electron energy, 250 mA electron current) of the LURE synchrotron facility (Orsay, France), using a double-crystal Si(311) monochromator with harmonic rejection and two ionization chamber detectors filled with a He–Ne mixture. The samples were mixed with boric acid (with careful control of the homogeneity), pressed into pellets of overall absorbance above the V K-edge $\simeq$ 2.0, and examined at low temperature using a liquid-N_2 cryostat. The acquisition of the spectra (5300–6300 eV, ΔE = 2 eV) was made using the "Quick-EXAFS" mode (*31*). The EXAFS data processing was made using the following steps: subtraction of pre-edge (combination of straight line and Victoreen function), approximation of the μ_0 background with a segment–spline baseline method, refinement of the baseline with multiple iteration averaging (checking that no components of significant frequencies were included in the subtracted baseline), and k^1- or k^3-weighted Fourier transform with Hanning windows. When necessary, selected peaks in R space were backtransformed and fitted to the standard single-scattering EXAFS expression. Backscattering amplitude and phase functions were extracted from spectra obtained with well-defined compounds: aqueous VO_4^{3-} for V–O pairs and V_2O_5 for V–V pairs (filtering in this last case the contribution appearing at R' = 2.73 Å in the phase-uncorrected Fourier transform of the spectrum).

RESULTS

X-ray Diffraction

Figure 2 presents the diffractograms obtained for the different specimens prepared: precursors, calcined samples, and crystalline pyrophosphate. The diffractograms of the last sample and of the VPAQ precursor show high degrees of crystallinity and agree well with those reported for $(VO)_2P_2O_7$ and $(VO)HPO_4 \cdot \frac{1}{2}H_2O$, respectively (*11*, *15*, *32*). The VPx precursors display only reflections corresponding to the $(VO)HPO_4 \cdot \frac{1}{2}H_2O$ phase, with a lower degree of crystallinity as evidenced by their broader and less intense diffraction peaks; there is a distinct increase in this effect for higher x values. This broadening is clearly less marked for those peaks due to diffraction by planes perpendicular to the layers (those with Miller index l = 0); the decrease of crystallinity thus mainly affects the order in the z direction, i.e., perpendicular to the layers of the structure.

In a similar way, the VPx-C-calcined samples show poor crystallinity. The only peaks detected can be ascribed to the $(VO)_2P_2O_7$ phase, and among them those with Miller index h = 0 show less severe broadening, indicating again a preferential decrease in crystallinity in the direction perpendicular to the layers in the structure, while the (200) reflection appears with particularly large

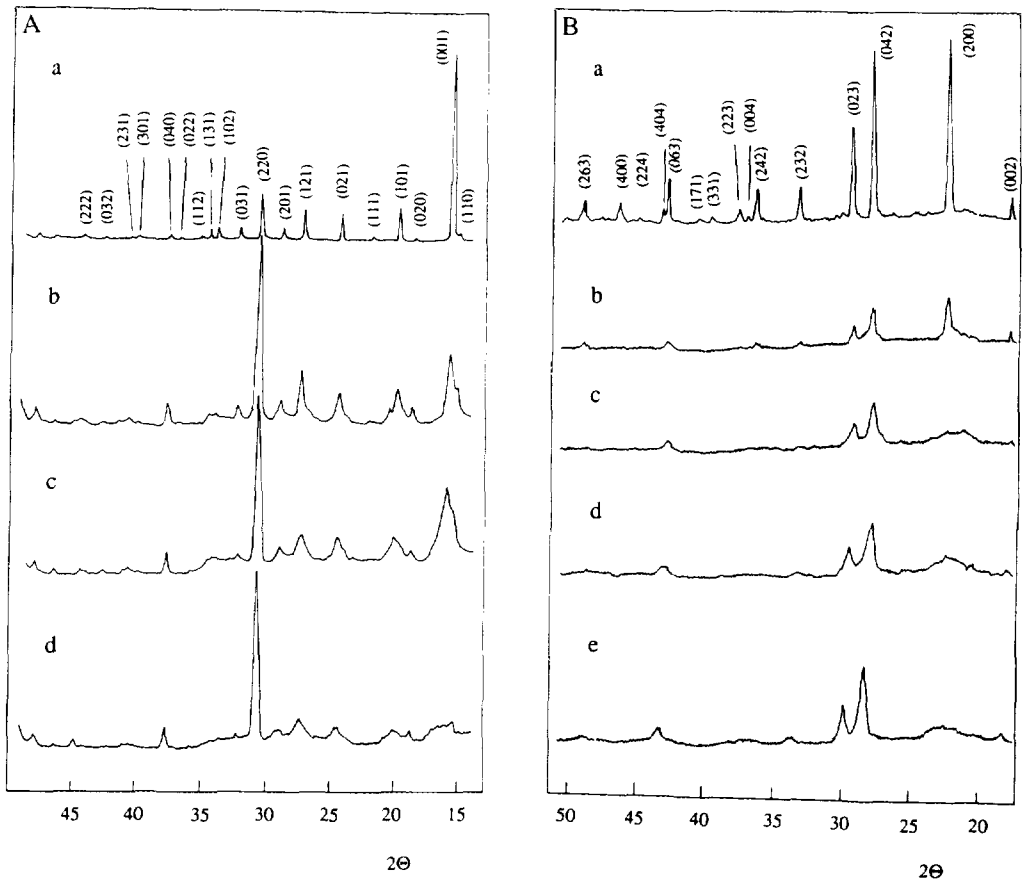

FIG. 2. XRD patterns of (A) precursors (a) VPAQ, (b) VP0.7, (c) VP1.0, (d) VP1.21; (B) (a) crystalline $(VO)_2P_2O_7$, and calcined samples (b) VPAQ-C, (c) VP0.7-C, (d) VP1.0-C, (e) VP1.21-C.

linewidth. Although it is more difficult to ascertain differences between the different VP*x*-C samples, there would seem to be a somewhat better crystallinity for those with larger *x* (compare, e.g., the region 33–40°). The VPAQ-C sample, prepared by the aqueous solvent route, shows also in the pyrophosphate structure a defect of crystallinity, but affecting all diffraction peaks to a similar extent, at variance with what was observed for the VP*x*-C specimens. It is interesting to observe that some tests of the precursor decomposition up to the same temperature under N_2, not under air, afforded materials almost completely amorphous in the case of VP*x* samples, while for sample VPAQ the pattern obtained (not shown), corresponding also to the $(VO)_2P_2O_7$ phase, displayed a crystallinity noticeably better than that of VPAQ-C.

Thermogravimetric Analysis

Figure 3 shows the weight loss curves, and their corresponding derivatives, obtained when the precursors are subjected to temperature-programmed heating in air. The vertical scale in this graph is normalized so that the starting point corresponds to the 100% level in all curves, these being subsequently shifted vertically for clarity of the representation. For all of them, five regions (designated I–V) can be observed. Region

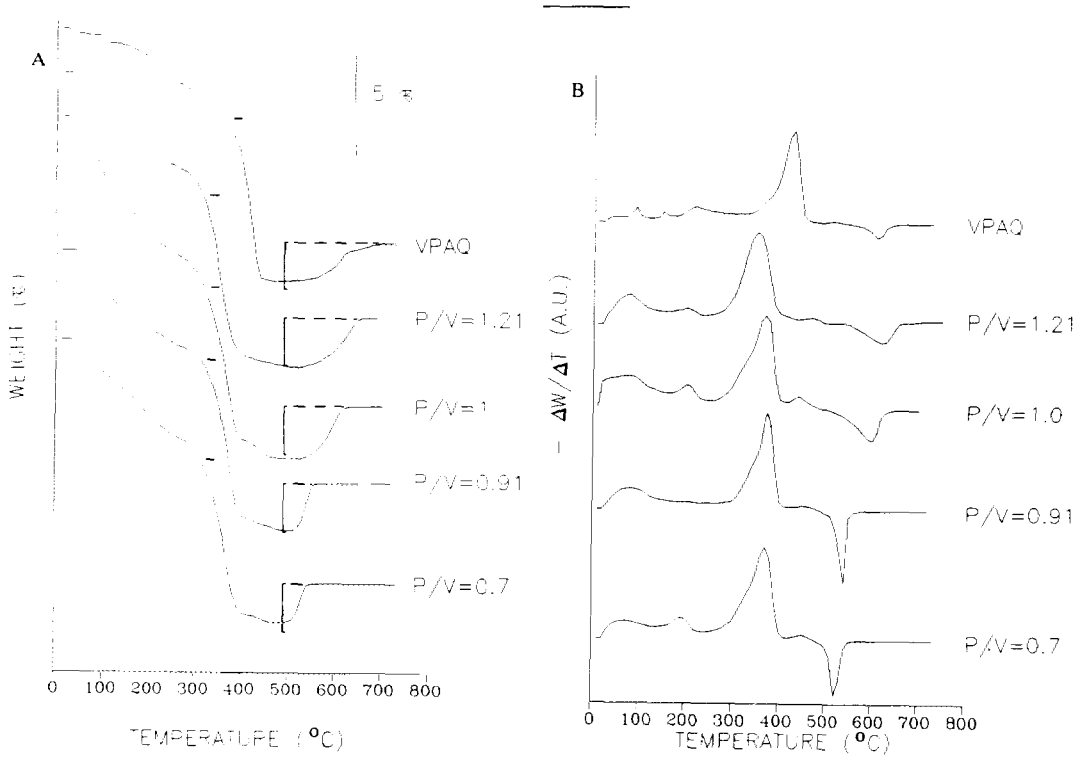

FIG. 3. (A) Weight loss curves for the calcination of precursor in air. (B) Derivative curves of previous weight loss curves.

I, for T below ca. 550 K, shows a more or less gradual decrease in weight, which probably corresponds to the loss of nonstructural water/solvent molecules; this process is not of great consequence for the objectives of this study and is not addressed in detail here. After that, region II occurs, located within the interval T = 620–720 K for the aqueous sample and T = 570–780 K for the organic samples, showing a distinctly steeper weight loss. Later, region III of relative weight stability is observed, followed by region IV of more or less steep weight increase, and finally, region V of constant weight.

X-ray diffraction examination of the materials obtained by interrupting the TG experiment during region III revealed only an ill-crystallized $(VO)_2P_2O_7$-type phase, as reported in the preceding section. For the material resulting at the end of the TG (region V), XRD data revealed in all cases only peaks corresponding to one or several of the known $VOPO_4$ phases, of which the δ-phase is first to appear (*11*). Peaks ascribable to phases of other compounds or stoichiometries (e.g., V_2O_5 or P_2O_5) were absen7t in all cases in these final products. These materials contained, as was shown by ESR spectroscopy, only very small amounts of V^{IV} species, so that their stoichiometries can be safely described as $VOPO_4$. It is therefore appropriate to express the observed weight differences as percentages referred to the weight of the corresponding $VOPO_4$ final state (and not to the weight of the initial state of the loaded samples since the stoichiometry is not uniform). A summary of the weight increases observed in region IV, together with the temperatures at which reactions proceed at peak rate within regions II and IV, is given in Table 1. We should recall that in Fig. 3 the bar representing a 5% weight change corresponds to taking as

TABLE 1

Temperatures of Main Weight Change Processes in TGA (Measured at the Peaks in the Derivative Curves) and Magnitudes of Weight Changes in TGA Region IV, for the Vanadium Phosphates Examined

	VP0.7	VP0.91	VP1.0	VP1.21	VPAC
ΔW (%)	2.0	2.4	2.7	2.5	1.9
T (II) (°C)	370	365	375	350	423
T (III) (°C)	522	538	600	628	610

[a] In interpreting the ΔW figures, one should remember that they are calculated assigning the 100% value to the product fully oxidized in region V, while the bar in Fig. 3 representing 5% weight change refers to the initial loaded sample.

100% the weight of the initial loaded sample. The weight changes can be compared with the values expected for different stoichiometric reactions such as

$$2(VO)HPO_4 \cdot \tfrac{1}{2}H_2O \rightarrow (VO)_2P_2O_7 + 2H_2O \quad (A)$$

$$(VO)_2P_2O_7 + \tfrac{1}{2}O_2 \rightarrow 2VOPO_4 \quad (B)$$

These reactions correspond to weight changes of -11.12 and $+4.94\%$, respectively (referred to the weight of the $VOPO_4$ final state). It is particularly interesting to note that in all cases the weight increase observed in region IV is substantially lower than that expected for reaction (B); in particular, for all VPx samples it is approximately half of it. This suggests that the redox state of vanadium in region III is nearly halfway between (+4) and (+5) [in agreement with the general behavior shown by chemical analysis of the $V^{IV}:V^{V}$ ratio for calcined phosphates of this kind prepared with different methods (*33*)] and that the stoichiometry of the process occurring in region IV is not that given in reaction (B) above, but more similar to

$$(VO)_2P_2O_{7.5} + \tfrac{1}{4}O_2 \rightarrow 2VOPO_4 \quad (C)$$

A vertical interval (thicker line) has been drawn in the curves of Fig. 3 to indicate in each case the weight change that would correspond to an oxidation starting from the $(VO)_2P_2O_{7.5}$ stoichiometry. On each curve a short horizontal mark has been drawn also, signaling the weight corresponding to the $(VO)HPO_4 \cdot \frac{1}{2}H_2O$ stoichiometry. This shows that the samples have, at the beginning of region II in the thermogravimetric curves, weights relatively close to those corresponding to that composition. Overall, the magnitudes of the weight changes observed in region II are therefore close to those that would occur for

$$2(VO)HPO_4 \cdot \tfrac{1}{2}H_2O + \tfrac{1}{4}O_2 \rightarrow (VO)_2P_2O_{7.5} + 2H_2O, \quad (D)$$

which could then be followed by reaction (C) in region IV to yield the final $VOPO_4$ product. This means that the VPx and VPAQ-C samples, which correspond to the material present in region III of the TGA curves, contain an excess of oxygen and an amount of V^{V} corresponding roughly to 50% of that expected for full oxidation of vanadium to the pentavalent state. This contrasts with their XRD diagram, which shows only peaks of the $(VO)_2P_2O_7$ phase.

On the other hand, these curves show that, while the process(es) occurring in region II takes place at temperatures relatively similar in all VPx samples (and ca. 50 K higher for sample VPAQ), the temperature necessary for the reaction occurring in region IV depends more strongly on the P : V ratio x used in the initial preparation mixture. In particular, the second process requires a rather lower temperature in the case of VPx samples with $x < 1.0$.

FT–IR Spectroscopy

Figure 4A presents the FT–IR spectra (range 1400–400 cm^{-1}) obtained for the different precursors. The observed bands coincide with those already reported for the hemihydrate compound (*34–38*) and assigned to its particular vibration modes (see Table 2). Only small differences can be noted among these spectra; the bands showing noticeable relative changes are those at positions 1135, 927, and 686 cm^{-1}, which appear in the VPx samples smaller or less

TABLE 2

Vibrational Frequencies (cm^{-1}) Measured with FT-IR in the 400–1400 cm^{-1} Range for the VPAQ Precursor and the Crystalline $(VO)_2P_2O_7$

$VOHPO_4 \cdot \frac{1}{2}H_2O$		$(VO)_2P_2O_7$	
416	δ(OPO)	423	$\delta(PO_4)$
483		514	
529		575	
548			
643	δ_{oop}(P—OH)	635	$\delta_{as}(PO_4)$
686	ω (coordinated H_2O)		
		745	ν_s(P—O—P)
		797	ν[V—(O=V)]
927	ν(P—OH)		
977	ν(V=O)	972	ν(V=O)
		1083	$\nu_{as}(PO_4)$
		1117	
1043	$\nu_{as}(PO_4)$	1146	
1104		1219	
		1245	
1135	δ_{ip}(P—OH)		
1200	$\nu_{as}(PO_2)$		

resolved. These bands are due either to P–OH groups or to water moelcules located in the interlayer space, indicating that the differences are related mostly to the interlayer connections.

The calcined samples display spectra similar to (but rather less resolved than) that of the well-crystallized pyrophosphate (Fig. 4B); this agrees with the indications of the XRD results. These bands have been previously reported (for real catalysts and for well-crystallized pyrophosphate) and assigned to modes of $(VO)_2P_2O_7$ as summarized in Table 2 (*17, 39, 40*). We should mention that a shoulder observable around 1105 cm^{-1} in the calcined samples may indicate the existence of some terminal P–OH groups, but its intensity, compared with that of the same peak observed in the precursors, shows that it cannot correspond to a substantial fraction of the phosphorus present. Also for the pyrophosphate phase there are particular vibrations associated with the links between the layers in the structure. Of these vibrations, the best resolved ones are those located at 797 and 745 cm^{-1}, ascribed respectively to [V—(O=V)] and [P—O—P]. A close examination of this spectral region reveals that, while the intensity of the 745 cm^{-1} band in the calcined samples is not much smaller than that measured in crystalline $(VO)_2P_2O_7$, the band at 797 cm^{-1} has diminished considerably in the calcined specimens (Fig. 5). The differences observed between the calcined samples for the other (main) peaks in the spectrum are proportionally less relevant.

ESR Spectroscopy

All precursors, as well as the calcined samples, display in the ESR spectra broad and nearly symmetric lines, without any splitting or resolved structure. The spectrum displayed by the crystalline $(VO)_2P_2O_7$ compound, although similar, is narrower and shows a more noticeable asymmetry. Some of these spectra are presented in Fig. 6. The spectrum of the well-crystallized pyrophosphate could be simulated numerically assuming Lorentzian lineshapes and a g tensor with orthorhombic symmetry. For the other samples, the larger linewidths made it impossible to resolve reliably any underlying asymmetry of the g tensor (only average g values could be determined meaningfully), but to reproduce the measured lineshape it was necessary to assume for the linewidths a marked anisotropy, at least to the level of axial symmetry. The best agreement between calculated and experimental spectra (shown in Fig. 6) was achieved with the ESR parameter values given in Table 3.

All the cited characteristics in the spectra correspond to magnetically concentrated V^{IV} species (most probably of vanadyl type in our case), in which the V^{IV}–V^{IV} magnetic interactions (either dipolar or of exchange type) obliterate the hyperfine splitting that is characteristic for V^{IV} in isolated situations, leading therefore to broad single lines. The smaller linewidths determined for the $(VO)_2P_2O_7$ sample indicate strong exchange interactions, which are known to occur in this compound (*41, 42*). Since in this highly concentrated material the linewidth will be determined mainly by the exchange-narrowing effect, the larger linewidths found for the calcined samples indicate that

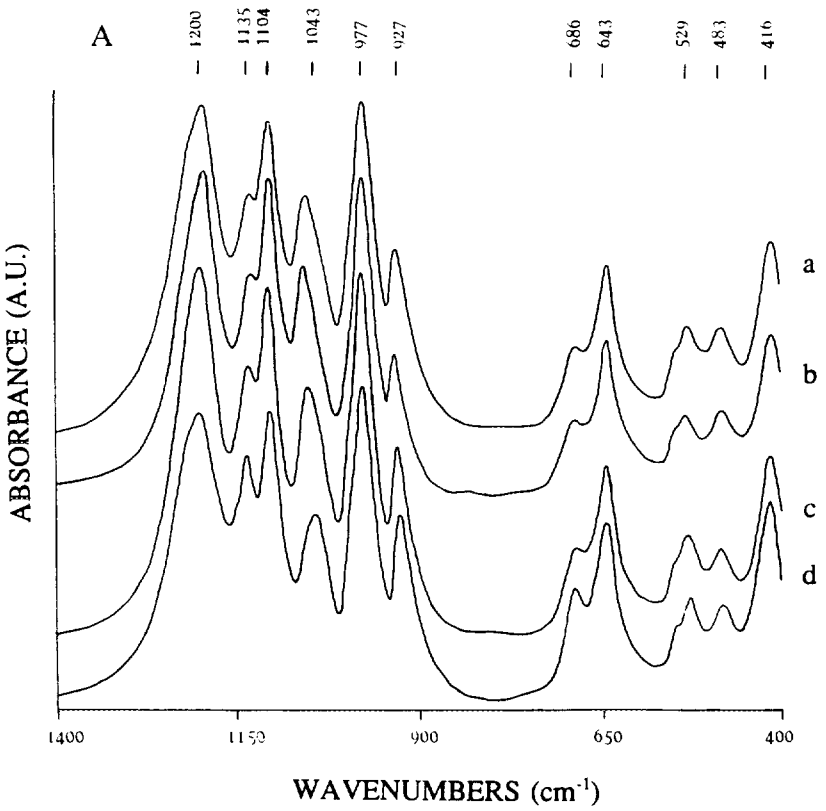

FIG. 4. (A) FT–IR of precursors (400–1400 cm^{-1}) (a) VP1.21, (b) VP1.0, (c) VP0.7, (d) VPAQ.

for these the V^{IV}–V^{IV} exchange interactions, if present, have magnitudes clearly smaller than those in the pure crystalline pyrophosphate.

EXAFS Data

In order to clarify better the disorder and nonstoichiometric characteristics of the calcined samples, X-ray absorption spectra were measured for several of them. The normalized EXAFS oscillations extracted from these spectra are presented in Fig. 7, which includes also the data measured in the same way for the crystalline pyrophosphate. Figure 8 gives the corresponding Fourier transforms (FTs); they are obtained without correction for backscattering phase and amplitude functions, so that the positions R' at which the peaks appear are lower (by displacements of 0.3–0.5 Å) than the true distances to the corresponding scatterers.

The amplitude of the oscillations is seen to decrease substantially for the VPx-C samples when x increases; this is reflected in the corresponding FTs. The first coordination shell, represented in the FT by the peak at R' = 1.4–1.5 Å, has in sample VP0.7-C an area similar to that in $(VO)_2P_2O_7$, but decreases for the other samples. Analysis of this shell is not easy in these materials, due to the large irregularity in the first shell distances: For the well-crystallized $(VO)_2P_2O_7$, the structure reported (*15*) reveals four different vanadium lattice positions, each one having different V–O coordination distances. The result is that the apical vanadyl V=O bonds vary in length between 1.53 and 1.73 Å, the equatorial single V–O bonds between 1.92 and 2.08 Å, and the axial V–O

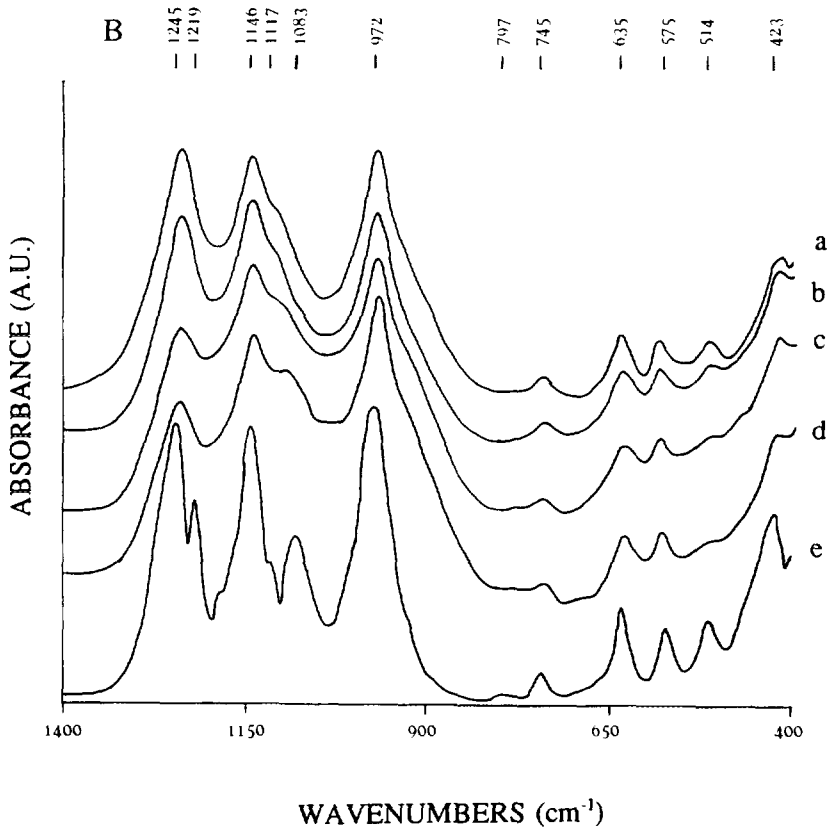

FIG. 4. (B) FT-IR of calcined samples (400–1400 cm^{-1}) (a) VP1.21-C, (b) VP1.0-C, (c) VP0.7-C, (d) VPAQ-C, (e) $(VO)_2P_2O_7$.

long bonds between 2.17 and 2.37 Å. Each of these distances may have its own Debye–Waller factor, which is in principle unknown; this makes it hard to obtain a good simulation of the spectra. In fact, the attempts to fit the filtered oscillations of the V–O shell in the $(VO)_2P_2O_7$ spectrum using models with a moderate number of different distances failed (for comparison, the same procedure was tried, and achieved successfully, in reproducing the V–O shell contribution in the spectrum of V_2O_5, which is much more regular in structure). Because of these difficulties, only qualitative differences in disorder levels, evidenced in the amplitudes of the corresponding contributions, can be asserted for the structure of the V–O shells in the VP*x*-C samples. We should mention that better resolved vanadium *K*-edge EXAFS spectra have been reported by Centi *et al.* (*43*) for $(VO)_2P_2O_7$ catalysts recrystallized by prolonged equilibration with a hydrocarbon–O_2 reaction mixture. In some cases two V–O contributions seem to appear resolved in the Fourier transform. However, few details were given about the acquisition and data reduction of these spectra. Thus it is not easy to ascertain the significance of the incipient peak separation observed by these authors in the V–O shell, especially since the spectra were obtained (seemingly at room temperature) with an in-house rotating anode source. This will result probably in a reduced signal-to-noise ratio. Another set of vanadium EXAFS data was reported by Vlaic and Garbassi (*44*) in this

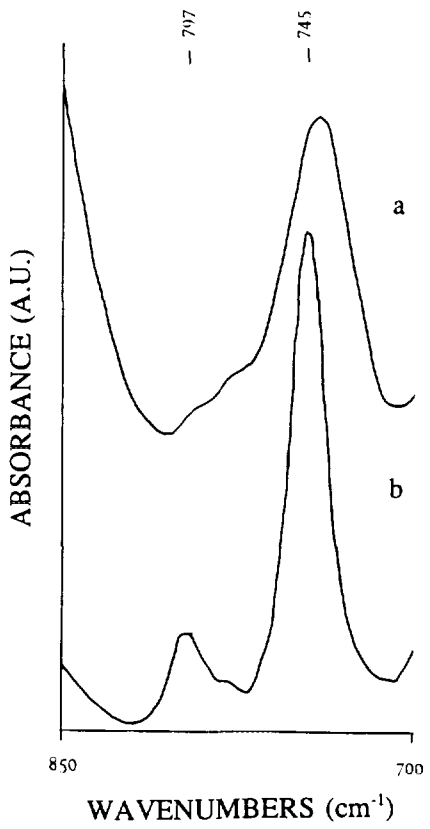

FIG. 5. FT-IR of calcined samples (700–850 cm^{-1}) (a) VP0.7-C and (b) $(VO)_2P_2O_7$.

type of system. The main conclusions of these authors were based on a two-shell fit of the V–O coordination. This seems questionable as it implies adjusting eight parameters, and the intervals seemingly used in those fits for k (7 $Å^{-1}$) and R (less than or equal to 1 Å) allow a maximum number of free parameters $N_{free} \approx 5$–6. In any case, that study was made on materials prepared through the aqueous method, so its results are not directly comparable with the data presented here.

The second-shell contribution was not observed in the VP1.0-C and VP1.21-C samples but were able to be analyzed easily in the sample VP0.7-C. Indeed an optimal fit of both the corresponding backtransformed oscillations and the Fourier transform module peak could be achieved assuming a vanadium scatterer and using parameters N = 1.15 neighbors, r = 3.09 Å, $\Delta\sigma = -0.0036$ $Å^2$, and $\Delta E = -3.6$ eV (Fig. 9). The N value agrees with a model of vanadium pairs, as corresponds to the structure of $(VO)_2P_2O_7$, although the V–V distance is shorter than the average value in the latter (3.19 Å), approaching that existing in V_2O_5 (3.08 Å). This may be related to the higher average oxidation state of vanadium in the calcined phosphate. However, in the case of the well-crystallized pyrophosphate the simulation with just a vanadium scatterer was not enough to simulate either the backtransformed oscillations or the Fourier transform module peak. This could indicate that some additional V–P contribution would be needed to reproduce adequately this part of the spectrum in the well-crystallized pyrophosphate and that the interference between V–V and V–P oscillations ultimately conditions the shape of the contribution due to the second coordination shell. Actually, a $(VO)_2P_2O_7$ crystalline specimen prepared by a different method afforded a much more depressed second coordination shell EXAFS contribution (*45*). An accurate analysis of this part of the spectrum could not be carried out because model compounds were not easily available. However, since there

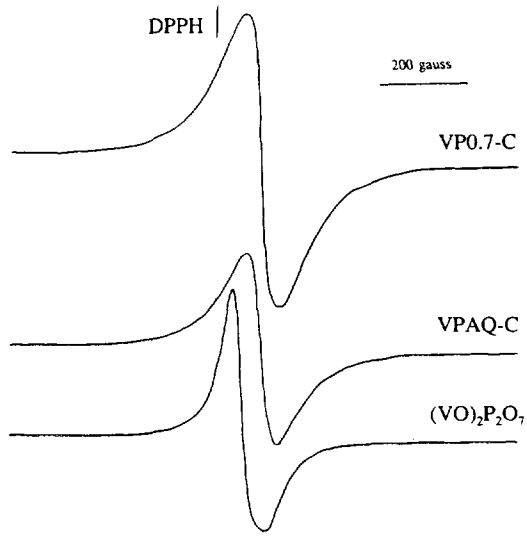

FIG. 6. ESR of calcined samples and $(VO)_2P_2O_7$.

TABLE 3

ESR Parameters (g Values and Peak-to-Peak Width ΔH) Obtained through Computer Simulation of the Experimental Spectra for the Well-Crystalized $(VO)_2P_2O_7$ and for VP0.7-C and VPAQ-C Samples

	g_i	$\langle g \rangle$	ΔH_i(G)
VPAQ-C	Not resolvable	1.96	$\Delta H_\perp = 715$, $\Delta H_\parallel = 133$
VP0.7-C	Not resolvable	1.96	$\Delta H_\perp = 295$, $\Delta H_\parallel = 630$
$(VO)_2P_2O_7$	$g_x = 1.983$ $g_y = 1.963$ $g_z = 1.938$	1.96	$\Delta H_x = 80$, $\Delta H_y = 150$, $\Delta H_z = 150$

does not seem to be any such interference in the VP0.7-C sample, we may conclude that the position of the phosphorus atoms is probably disordered in this sample to an extent enough to suppress their effect in the EXAFS spectra. In the VP1.0-C and VP1.21-C, this disorder apparently affects also the V–V distance, so that no second coordination shell contribution was observable at all.

On the other hand, the peak appearing at $R' \simeq 3.9$ Å in the FT for sample VP0.7-C is clearly displaced from the position $R' = 3.37$ Å (next shell observed in $(VO)_2P_2O_7$). The latter corresponds undoubtedly to the V–V distance of 3.86 Å in the V–(O=V) arrangement perpendicular to the layers, in which multiple scattering contributions, large in this case because of the colinear geometry (lens effect), must enhance

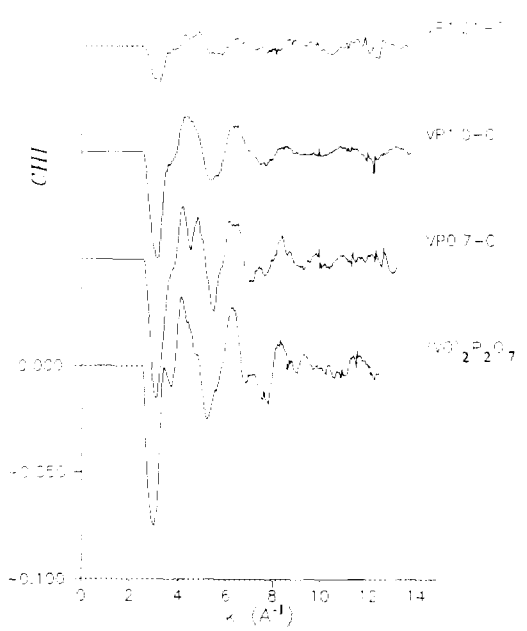

FIG. 7. EXAFS oscillations on the V K-edge of calcined samples and of $(VO)_2P_2O_7$.

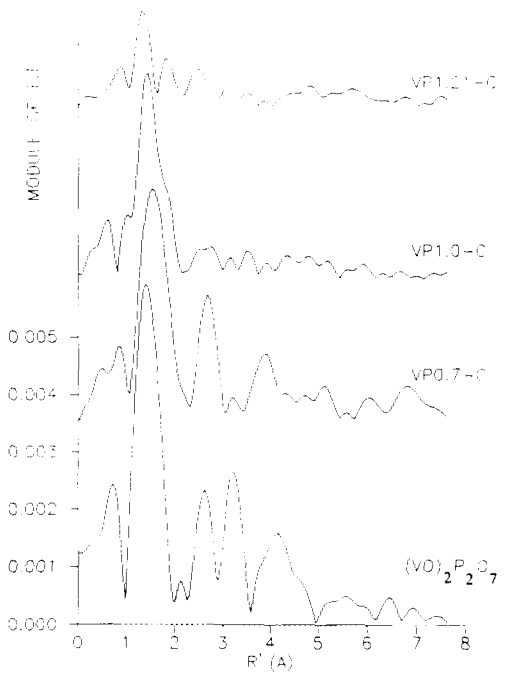

FIG. 8. Magnitude of the Fourier transform (k^1 weighted) for the EXAFS data in Fig. 7.

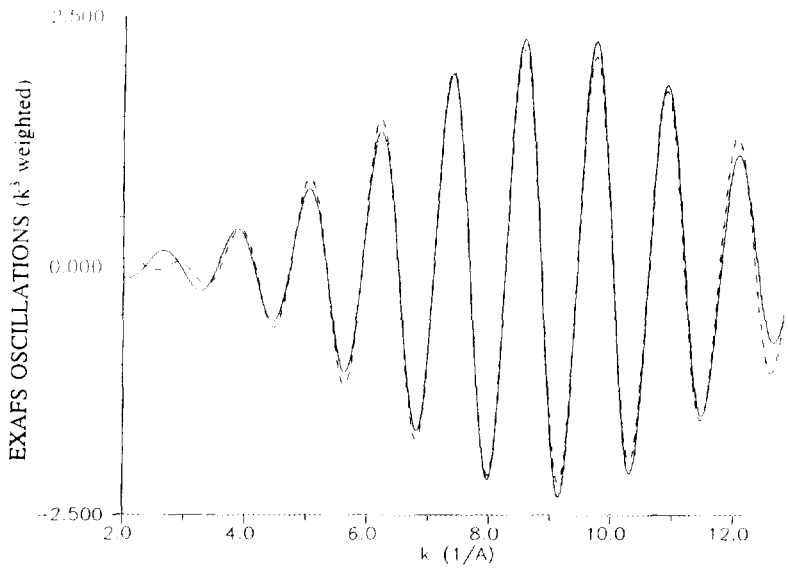

FIG. 9. EXAFS oscillations, backtransformed from the FT range R' = 2.3–3.1 Å, for the calcined sample VP0.7-C (—); together with (---) simulated curve (see text).

strongly the contribution to the spectrum. Therefore it would seem that, at least locally, an increase is produced in the distance between the V ions of adjacent layers for sample VP0.7-C. However, it would not be appropriate to attempt a least-squares fitting of this contribution with the standard single-scattering formulation, since the cited lens effect is likely to be present here also.

For samples with x = 1 and 1.21, the absence of any higher shell contributions, together with the already discussed substantial decrease in the intensity of the first-shell features, indicates clearly a higher degree of local disorder around the vanadium atoms, which increases with x and affects the V–O, V–V, and (probably also) V–P distances. Therefore, apart from the observation of this substantial increase in disorder around vanadium, further quantitative analysis of the EXAFS spectra does not seem appropriate for these samples.

DISCUSSION

Structural Aspects of the Nonstoichiometry

The TGA results indicate clearly that vanadyl phosphates of this type, when obtained by calcination in air at temperatures in the vicinity of 700 K, contain V^V and V^{IV} ions even though XRD shows only the V^{IV}-related phase; this is common to all the different preparations examined here. Such behavior of V–P–O samples has been reported before (*17, 21, 22*), but those works did not give much relevance to the high level of nonstoichiometry that, as shown above, can be accommodated in the phase concerned. The existence of a compound with this intermediate $(VO)_2P_2O_{7.5}$ stoichiometry was reported some time ago by Bordes and Courtine (*46*). These authors, however, obtained it only in near equilibrium conditions, for temperatures above 1000 K and partial pressures of $O_2 \leq 0.1$ atm. They interpreted this structure as a "hybrid crystal" made of "microdomains" of VPO_5 and $VPO_{4.5}$ phases, but did not report for it any XRD data. In our case this stoichiometry resulted, with apparent stability, under different temperatures and O_2 partial pressure. Perhaps this phase appears as a metastable state, made possible in our experiments by kinetic constraints rather than for thermodynamic reasons. The fact is that our results show the possibility of producing, during

the practical preparation of catalysts, a solid with the XRD of a vanadyl pyrophosphate-type structure but with a definite $(VO)_2P_2O_{7.5}$ stoichiometry. We do not think that this mixed redox state can be ascribed simply to the presence of some unidentified V^V-containing amorphous phase coexisting with $(VO)_2P_2O_7$; in such a case the ESR spectra of the calcined samples should have presented a narrower signal due to the V^{IV}–V^{IV} exchange interactions of $(VO)_2P_2O_7$. On the contrary, the broad signal detected indicates that the exchange interaction expected for V^{IV}–V^{IV} pairs is substantially suppressed. This fact has an important implication since strong exchange interactions exist in the $(VO)_2P_2O_7$ structure not only between the two V ions in an octahedron pair (with coupling constant $J/k_B = -65.7$ K), but also between V ions of octahedra adjacent in the direction of the *b* axis and connected through two O–P–O links (giving $J/k_B = -46$ K). These interactions produce linear magnetic chains of magnetically coupled V^{IV} ions along axis *b* (*41*, *42*). The strong reduction of exchange in the calcined materials studied here suggests the possibility that the V^V and V^{IV} ions are located in an alternating way in these chains, i.e., with a disposition

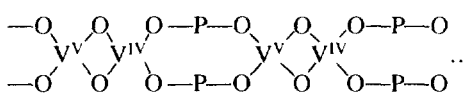

This would allow each V^{IV} ion to have only V^V ions as immediate neighbors in the chain and thus to experience no exchange interactions within it. In this respect it may be worthwhile to recall that the reported $(VO)_2P_2O_7$ structure contains vanadyl bonds of two distinct lengths (respectively around 1.54 and 1.72 Å), ordered along the *b* axis precisely in the same alternating way. It may well be that this characteristic helps in stabilizing the cited coupling and ordering of V^V and V^{IV} ions.

To summarize, all the data point to the presence, in the calcined materials, of a situation in which V^V–V^{IV} mixed-valent pairs exist, constituting an intermediate redox state that might well have a definite degree of stability in the preparative conditions used. Indeed, this mixed-valence state is already considered to exist in oxo-linked vanadyl pairs having particular stability when the V=O are oriented mutually antiparallel in the pair (*47*) as is the case in the $(VO)_2P_2O_7$ structure.

The question that now arises is that if such mixed valency can exist within the pyrophosphate lattice, where in the structure should the extra oxygen necessary to complete the stoichiometric composition be located? One possibility for this would be that the new oxygen atoms would enter the lattice by breaking the pyrophosphate links to give phosphate groups

$$O_3P\text{–}O\text{–}PO_3^{-4} + [O] + 2e^- \rightarrow 2PO_4^{-3} \quad \text{(E)}$$

However, the IR results show that the P–O–P vibrations have not been suppressed to the extent (ca. 50%) that would be expected if this mechanism were correct. IR does indicate that some amount of terminal P–OH residues may exist, but they might correspond to the termination of the structure at the surface. The phosphorus *K*-edge EXAFS data reported by Garbassi *et al.* (*48*) also failed to give any clear information about the catalyst structure; this type of data seemed sensitive only to the immediate tetrahedral environment of the P atom, which is preserved in any case. Since the first step of the reaction of the O_2 molecule on the material is likely to involve a direct V^{IV}–O_2 interaction (to achieve the necessary electron transfer), we could imagine also a second possibility, namely, that the additional oxygen atoms are inserted between two vanadium ions of a pair

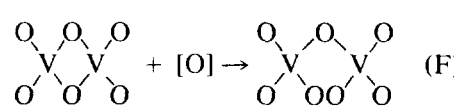

This does not seem likely if it is assumed that both γ- and δ-$VOPO_4$ phases, which are those appearing as initial full oxidation products, still have, as proposed in the liter-

ature, these octahedron pairs. Although this assumption has been recently challenged (*49*), we still can rule out such a hypothesis (F). As a matter of fact, the EXAFS data indicate that the integrity of the V–V pairs is preserved at least in one of the samples that presents the mixed stoichiometry state (VP0.7-C). The intercalation of oxygen between two V atoms could take place anyway, however, if these belonged to different layers and the oxygen atom remained intercalated between them, i.e., if the vanadyl–vanadyl contacts along axis *a* of the lattice were affected according to a scheme such as

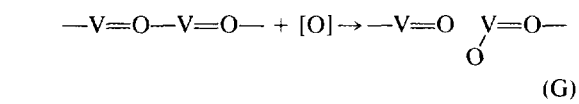

(G)

This type of interaction could then explain both the lesser intensity of the V=O—V vibration band in the FT–IR spectrum and the detection of a peak, in the EXAFS–FT curve obtained for sample VP0.7-C, at a distance longer than that due to V=O—V distances in crystalline $(VO)_2P_2O_7$. It is worth noting that this model does not conflict with the isotopic studies of Abdelouahab *et al.* (*49*), which show that in the oxidation of $(VO)_2P_2O_7$ to $VOPO_4$ the oxygen added from the gas phase ends up incorporated in the breaking of the P–O–P links and of the $V(O)_2P$ pairs; such breaking (with the corresponding incorporation of the O atoms intercalated between the layers) might occur only in the second stage of oxidation (region IV of TGA).

The generation of the cited mixed V^{IV}–V^{V} state, with extra oxygen inserted in the structure, seems to be completed during region II of the TGA curves. In all these curves, a single main derivative TGA peak is observed in this region; this indicates that the dehydration and partial V oxidation reactions occur associated. This could happen through a consecutive mechanism in which the first rate-determining step is the elimination of the first interlayer H_2O molecule and the rest of the process (oxygen insertion included) follows on quickly as soon as room is made between the layers by the departure of H_2O. For the VPAQ sample the higher temperature at which this process occurs might then be origin for the somewhat higher average oxidation degree of vanadium, which results in this case. The transformation would end with the collapse of the interlayer space trapping an oxygen atom inside in the neighborhood of the vanadium atom and the "gluing" of the layers with P–O–P bonds. Even with such excess oxygen included between the layers, the overall topology of the pyrophosphate lattice might be preserved with negligible change in lattice parameters; the dimension of the framework may well be determined by the sizes of the elemental "bricks" in the structure (the double vanadium octahedra) and of the links between them (the pyrophosphate bridges). Therefore, the positions of the reflections observed in XRD might remain unchanged.

Effects of Different Preparation Methods in the Structure of Precursors and Catalysts

Using aqueous or organic solvents in the preparation of the materials brings as a first difference a change in crystallinity of the hydrated precursors. The preferential broadening, observed for the VP*x* samples, of the XRD peaks corresponding to directions not parallel to the layer planes could be due, at least in part, to a smaller dimension of the crystallites in the *a* direction. This could imply that the alcohol solvent might induce a larger relative crystal growth rate in the directions parallel to the layers. There are, however, indications in the FT–IR spectra (where bands ascribed to P–OH and H_2O modes decrease) that the interlayer regions inside the crystallites are also affected by the use of organic solvents. This is consistent with the well-known ability of these hydrated phosphates to occlude intercalated organic molecules in the interlayer space (*8, 17, 50*). Local distortions in the layers, induced by the bulkier alcohol molecules, would contribute then also to the

decrease in crystallinity observed. These distortions would not be very large; the structure of the bonds within the layers themselves seems much less affected by the use of organic solvent in the preparation, in view of the negligible changes in the IR peaks related to those bonds.

In respect to the vanadyl pyrophosphate, the burning and elimination of these organic species during calcination may contribute to produce breaks in the solid structure. This would be ultimately responsible for the high crystalline disorder observed usually (and in this work) in V–P–O catalysts prepared in this way, according to the ideas prevalent in the literature (*17, 19, 20*). The connections between the layers are likely to be more affected than the structure of the layers themselves (already fully formed in the precursor), and accordingly the loss of crystallinity is manifested by XRD more severely in the directions perpendicular to the layers. It is also likely that the irregularities in the interlayer space induced by the occluded molecules may affect the kinetics of the dehydration/vanadium oxidation process: This agrees with TGA results showing that the corresponding temperature is ca. 50 K lower for the VP*x* samples.

Effects of the P : V Ratio Used in Catalyst Preparation

In principle, the similarity in the FT–IR spectra of several VP*x* precursors and in the details of their dehydration shown by TGA would suggest that they have very similar characteristics of reticular bond strength and chemical reactivity. It is, therefore, somewhat surprising that the chemical behavior of the resulting VP*x*-C specimens appears clearly as *x*-dependent. This effect is observed in the TGA data, which show that changes in the full oxidation to $VOPO_4$ proceeds at lower temperature for samples with lower *x*. The literature also reports changes in catalytic activity for selective oxidation of V–P–O materials when they are prepared with varying P : V ratios. These changes have been sometimes ascribed to differences in composition of the external surface, influencing the surface reactivities (*23–29*). In our case, at least, this cannot be the only difference between these materials, as shown clearly by the EXAFS spectra, which reveal a higher local disorder for higher *x* values.

Since the full oxidation of the pyrophosphate structure has, as its main first process, the penetration of O_2 between the layers, which proceeds to break them completely apart, the TGA behavior of the different samples then would suggest that for the higher *x* values the connections between layers could be better established. This would mean that, for $x > 1$, the array of P–O–P bridges between layers might be more dense and regular, rendering the O_2 penetration more difficult and giving in the calcined specimens a pyrophosphate lattice that would be more regular (at the medium- and long-range scales) and better defined in XRD. The more regular P–O–P bridge array would provide at the same time less room and flexibility to accommodate in the optimum position the excess oxygen incorporated during dehydration, so that the geometries would be much more distorted at the local (atomic) scale, resulting in less-defined features around the vanadium in the EXAFS spectrum. Conversely, in samples prepared using lower P : V initial ratio there could be more defects at the phosphate positions, giving a somewhat worse regularity of P–O–P bridges, which would allow the bonds around vanadium to relax locally toward more uniform values while making the reaction with O_2 easier. It is noteworthy that in such a model a *higher* degree of local distortion (as achieved in the samples with higher *x*) would be accompanied by a *higher* crystalline regularity and a *higher* resistance to full oxidation to $VOPO_4$ (but without making difficult the generation of a mixed V^{IV}–V^{V} state!). Perhaps all these characteristics help to make the catalysts better when prepared with higher P : V ratios, as widely recognized in the literature. This model, however, would need further work to assess its validity.

CONCLUSIONS

The physicochemical techniques used to characterize the different vanadium phosphate samples prepared have provided information on several details of the structure and reactivity of the intervening phases. The clearest result is that, in the materials obtained by calcination at temperatures similar to those used in preparation of real catalysts, there is a definite tendency to have mixed-valence V^{IV}–V^{V} pairs that are generated in a cooperative topotactic dehydration–oxidation process and are distributed in an alternating manner along the *b* direction of the pyrophosphate. The corresponding excess oxygen remains trapped between the layers of the $(VO)_2P_2O_7$ structure, disrupting mainly the interlayer V=O–V=O contacts and contributing probably to the crystallization deficiency observed.

Another observation in this work that agrees with previous work in the literature is the more disordered crystalline structure appearing in the fresh catalyst when organic solvent is used in the preparation. The disorder may affect not only the (long-range) stacking of the structural layers but also the (short-range) vanadium environment in the catalysts. It seems likely that both disorders are favored by the occlusion of organic molecules within the structure during the preparation and that their magnitude will be influenced by the initial P/V ratio. An additional consequence of this is that the dehydration in air may take place at a lower temperature than in the aqueous preparation; this in turn helps to prevent an excessive oxidation of vanadium (beyond the level of 50% V^{V}) resulting in a higher stability of the pyrophosphate phase.

It is important to bear in mind that these conclusions refer to the solids resulting from the catalyst preparation process, before any contact with the reaction mixture. The reaction conditions may well give rise to changes in the state or in the structure of the catalysts. Indeed, it has been shown that after several hundred hours of operation, the catalysts become much better crystallized, as evidenced by XRD (*51*) and that the average redox state of the vanadium in the recovered material can be rather close to 4.0 (*43*). This means that the excess of oxygen and the accompanying lattice distortions may be absent, or rather reduced, during reaction.

We think, however, that the results of our work still have relevance for the understanding of this system. First, they may help us to understand several aspects of the catalyst preparation process, which is known to have a large influence on the final catalytic activity. Second, they make clear that the observation of XRD peaks corresponding to the $(VO)_2P_2O_7$ phase is compatible with a substantial oxidation of vanadium in this phase. The third feature of interest is the particular stability that the V^{IV}–V^{V} mixed-valence pairs seem to have in the $(VO)_2P_2O_7$ structure. This means that one should consider the possibility that such pairs exist during reaction at the surface of well-crystallized catalysts (even if its bulk structure contained only V^{IV}), and that they may play a specific role in the reaction mechanism. Unfortunately, the detection of such pair structure at the surface is not easy to achieve; the ESR spectra, for example, would be dominated by the signal from the bulk V^{IV} ions.

ACKNOWLEDGMENTS

M.L.G. and M.F.G. thank Ministerio de Educacion y Ciencia from España for the PFPI fellowships with which they participated in the present research. Thanks are given also to Dr. J. M. Palacios, for the SEM/EDAX analysis of catalyst samples, and to the EC Large Scale Installations Programme for facilitating access to the LURE synchrotron.

REFERENCES

1. Martin, A., Lücke, B., Seeboth, H., and Ladwig, G., *Appl. Catal.* **49,** 205 (1985).
2. Martin, A., Lücke, B., Seeboth, H., Ladwig, G., and Fisher, E., *React. Kinet. Catal. Lett.* **38,** 33 (1989).
3. Amorós del Toro, P. J., Ph.D. thesis, Universitat de Valencia, 1989.
4. Ai, M., *J. Catal.* **101,** 389 (1986).
5. Ai, M., *J. Catal.* **101,** 473 (1986).
6. Hodnett, B. K., *Catal. Rev. Sci. Eng.* **27,** 373 (1985).

7. Centi, G., Trifirò, F., Ebner, J. R., and Franchetti, V. M., *Chem. Rev.* **88,** 55 (1988).
8. Arnold, E. W., and Sundaresan, S., *Appl. Catal.* **41,** 225 (1988).
9. Bosch, K., Bruggink, A. A., and Ross, J. R. H., *Appl. Catal.* **31,** 323 (1987).
10. Van Geem, P. C., and Nobel, A. P. P., *Catal. Today* **1,** 5 (1987).
11. Bordes, E., *Catal. Today* **1,** 449 (1987).
12. Contractor, R. M., Bergna, H. E., Horowitz, S. H., Blackstone, C. M., Malone, B., Torardi, C. C., Griffiths, B., Chowdhry, U., and Sleight, A. W., *Catal. Today* **1,** 49 (1987).
13. Cavani, F., Centi, G., Riva, A., and Trifirò, F., *Catal. Today* **1,** 17 (1987).
14. Centi, G., López, Nieto, J. M., Ungarelli, F., and Trifirò, F., *Catal. Lett.* **4,** 309 (1990).
15. Gorbunova, Y. E., and Linde, S. A., *Dokl. Akad. Nauk SSSR.* **279,** 585 (1979).
16. Centi, G., Trifirò, F., and Poli, G., *Appl. Catal.* **19,** 225 (1985).
17. Busca, G., Cavani, F., Centi, G., and Trifirò, F., *J. Catal.* **99,** 400 (1986).
18. Bordes, E., Courtine, P., and Johnson, J. W., *J. Solid State Chem.* **55,** 270 (1984).
19. Horowitz, H. S., Blackstone, C. M., Sleight, A. W., and Teufer, G., *Appl. Catal.* **38,** 193 (1985).
20. O'Connor, M., and Hodnett, B. K., *Appl. Catal.* **42,** 91 (1988).
21. Vlaic, G., and Garbassi, F., *J. Catal.* **122,** 312 (1990).
22. Martini, G., Trifirò, F., and Vaccari, A., *J. Phys. Chem.* **86,** 1573 (1982).
23. Garbassi, F., Bart, J. C. J., Montino, F., and Petrini, G., *Appl. Catal.* **16,** 271 (1985).
24. Satsuma, A., Kattori, A., Furuta, A., Miyamoto, A., Hattori, T., and Murakami, Y., *J. Phys. Chem.* **92,** 2275 (1988).
25. Hodnett, B. K., Permanne, P. H., and Delmon, B., *Appl. Catal.* **6,** 231 (1983).
26. Zazhigalov, V. A., Belousov, V. M., Komashko, G. A., Pyataniskaya, A. I., Merkureve, Y. N., Poznyakevich, A. L., Stoch, J., and Haber, J., *in* "Proceedings, 9th International Congress on Catalysis, Calgary, 1988" (M. J. Phillips and M. Ternan, Eds.), Vol. 5, p. 1635. Chem. Institute of Canada, Ottawa, 1988.
27. Zazhigalov, V. A., Belousov, V. M., Komashko, G. A., Pyayniskaya, A. I., Goldenburg, G. I., and Konovalova, N. D., *React. Kinet. Catal. Lett.* **37,** 71 (1988).
28. Yamazoe, H., Morishige, H., and Terakoa, Y., *Stud. Surf. Sci. Catal.* **14,** 15 (1988).
29. Haas, J., Plog, C., and Manuz, W., *in* "Proceedings, 9th International Congress on Catalysis, Calgary, 1988" (M. J. Phillips and M. Ternan, Eds.), Vol. 4, p. 1632. Chem. Institute of Canada, Ottawa, 1988.
30. Conesa Cegarra, J. C., Ph.D. thesis, Universidad Complutense de Madrid, 1977.
31. Prieto, C., Parent, P., Le Normand, F., Lagarde, P., and Dexpert, H., *in* "Proceedings, 2nd Conference on Progress in X-ray Synchrotron Radiation Research, Roma, 1989" (A. Balerna, E. Bernieri, and S. Mobilio, Eds.), p. 563. SFI-Editrice Compositori, Bologna, 1990.
32. Johnson, J. W., Johnston, D. C., Jacobson, A. J., and Brody, B. F., *J. Am. Chem. Soc.* **106,** 8123 (1984).
33. Conesa, J. C., and López Granados, M., in preparation.
34. R'Kha, C., Vanderborre, M. T., Livage, J., Prost, R., and Huard, E., *J. Solid State Chem.* **63,** 202 (1986).
35. Amorós, P., Ibañez, R., Martínez Tamayo, E., and Beltrán Porter, A., *Mater. Res. Bull.* **24,** 1347 (1989).
36. Villeneuve, G., Abdelhaker, E., Beltrán, D., Drillar, M., and Hagenmuller, P., *Mater. Res. Bull.* **21,** 621 (1986).
37. Labonette, D., and Taravel, B., *J. Chem. Res.* **34** (1984).
38. Bucovec, P., Millićev, S., Demšar, A., and Golić, L. J., *J. Chem. Soc. Dalton Trans.*, 1802 (1981).
39. Ramis, G., Busca, G., Lorenzelli, V., La Ginestra, A., Galli, P., and Masucci, M. A., *J. Chem. Soc. Dalton Trans.*, 881 (1988).
40. Bordes, E., Ph.D. thesis, Compiègne, 1979.
41. Johnston, D. C., Johnson, J. V., Goshom, D. P., and Jacobson, A. J., *Phys. Rev. B* **35,** 219 (1987).
42. Beltrán Porter, D., Amorós, P., Ibañez, R., Martínez, E., Beltrán Porter, A., Le Bail, A., and Ferrey, G., *Solid State Ionics* **32/33,** 57 (1989).
43. Centi, G., Trifirò, F., Busca, G., Ebner, J., and Gleaves, J., *Faraday Discuss. Chem. Soc.* **87,** 215 (1989).
44. Vlaic, G., and Garbassi, F., *J. Catal.* **122,** 312 (1990).
45. López Granados, M., Conesa, J. C., Fernández-García, M., and Prieto, C., *in* "Proceedings, 6th International Conference on X-Ray Absorption Fine Structure, York, 1990" (S. Samar Hasnain, Ed.), p. 496. Ellis Horwood, London, 1991.
46. Bordes, E., and Courtine, P., *J. Catal.* **57,** 236 (1979).
47. Young, C. G., *Coord. Chem. Rev.* **96,** 89 (1989).
48. Garbassi, F., Bart, J. C. J., Tassinari, R., Vlaic, G., and Lagarde, P., *J. Catal.* **98,** 317 (1986).
49. Abdelouahab, B. F., Olier, R., Guilhaume, N., Lefebvre, F., and Volta, J. C., *J. Catal.* **134,** 151 (1992).
50. Alagna, L., Prosperi, T., and Tomlimson, A. G., *Mater. Res. Bull.* **22,** 691 (1987).
51. Cornaglia, L. M., Caspani, C., and Lombardo, E. A., *Appl. Catal.* **74,** 15 (1991).